ISSN 1063-7729, Astronomy Reports, 2013, Vol. 57, No. 11, pp. 818–832. © Pleiades Publishing, Ltd., 2013.
Original Russian Text © O.V. Kochina, D.S. Wiebe, S.V. Kalenskii, A.I. Vasyunin, 2013, published in Astronomicheskii Zhurnal, 2013, Vol. 90, No. 11, pp. 892–906.

Modeling of the Formation of Complex Molecules in Protostellar Objects

O. V. Kochina[1*], D. S. Wiebe[1], S. V. Kalenskii[2], and A. I. Vasyunin[3]

[1] *Institute of Astronomy, Russian Academy of Sciences, 48 Pyatnitskaya St., Moscow, 119017 Russia*

[2] *Astro Space Center, Lebedev Physical Institute, Russian Academy of Sciences, Pushchino, Moscow oblast, Russia*

[3] *Department of Astronomy, University of Virginia, Charlottesville, USA; Visiting scientist, Ural Federal University, Yekaterinburg, Russia*

Received May 29, 2013; in final form, June 11, 2013

Abstract—The results of molecular composition modeling are presented for the well studied low-mass star-forming region TMC-1 and the massive star-forming region DR21(OH), which is poorly studied from a chemical point of view. The column densities of dozens of molecules, ranging from simple diatomic to complex organic molecules, are reproduced to within an order of magnitude using a one-dimensional model for the physical and chemical structure of these regions. The chemical ages of the regions are approximately 10^5 years in both cases. The main desorption mechanisms that are usually included in chemical models (photodesorption, thermal desorption, and cosmic-ray-induced desorption) do not provide sufficient gas-phase abundances of molecules that are synthesized in surface reactions; however, this shortcoming can be removed by introducing small amount of reactive desorption into the model. It is possible to reproduce the properties of the TMC-1 chemical composition in a standard model, without requiring additional assumptions about an anomalous C/O ratio or the recent accretion of matter enriched with atomic carbon, as has been proposed by some researchers.

DOI: 10.1134/S1063772913110036

1. INTRODUCTION

One of the main difficulties in studying star formation is that this process can hardly ever be observed directly. To determine the conditions for star formation, indirect methods enabling estimation of the key physical parameters of this process based on observational data are used. Chemical modeling is an especially versatile diagnostic tool; in combination with spectral observations, it provides a way to estimate the evolutionary stage of a protostellar object. Furthermore, it is necesary to know the molecular composition of the studied region to more accurately determine the contributions of atoms and molecules to the thermal balance of matter and to estimate the efficiency of the interaction between matter and magnetic fields, provided that we know the degree of ionization.

It is generally believed that different evolutionary stages of protostellar objects are associated with different molecular tracers. For example, the main molecules that are observed in the prestellar core stage are CO, HCO^+, CS (the envelope), N_2H^+, N_2D^+, NH_3, H_2D^+, D_2H^+, and D_3^+ (the core). In this stage, the chemical composition is determined by the freezing-out of most molecules onto dust particles [1]. Class 0 protostellar objects are identified by the presence of spectral lines of N_2H^+, NH_3 (envelopes), H_2O, SiO, CH_3OH, SO (outflows), and complex organic compounds (hot cores). In this case, the molecular composition is explained by the evaporation of dust mantles accompanied by the ejection of complex molecules that have been synthesized on dust grains into the gas phase [2–5].

Astrochemical modeling is becoming a standard approach to explaining spectral observations of both individual protostellar objects and entire star-forming regions. However, uncertainties in the external and internal parameters of a chemical model can hinder the ability to draw of reliable conclusions. One important criterion for a model to be adequate is its ability to simultaneously describe the evolution of an appreciable number of molecules—both simple molecules consisting of two or three atoms and more complex ones, with high or low abundances.

*E-mail: okochina@inasan.ru

Information about the concentrations of a large number of molecules in a given object can be obtained from spectral surveys based on high-resolution spectral observations in a wide frequency range. A large number of lines associated with dozens of molecules, including both simple and complex compounds, are observed simultaneously in such spectral surveys. Unfortunately, the flip side of the wide frequency range is that, as a rule, we can only study one position towards a single object of interest at a time. Therefore, abundances estimated using spectral surveys generally correspond to some average molecular composition of the object, which complicates their comparison with chemical modeling results. Nevertheless, the fitting of observations is not possible without this modeling.

In this paper, we present astrochemical modeling results for two star-forming regions in different evolutionary stages—TMC-1 and DR21(OH)M—in which column densities of dozens of molecules have been measured. Section 2 describes the model used. Sections 3 and 4 are devoted to the modeling results for TMC-1 and DR21(OH)M, respectively. Section 5 discusses the conclusions drawn from our study.

2. THE MODEL OF A PROTOSTELLAR OBJECT

The "Presta" multi-point model for the chemical evolution of prestellar and protostellar objects that was used in this work has been developed at the Institute of Astronomy of the Russian Academy of Sciences since 1994 [6–8]. Its current version enables modeling of the collapse of a spherically symmetric core irradiated by both external, diffuse radiation and a central source (protostar) with given parameters [9, 10]. The region studied is divided into concentric cells, in each of which the dust temperature, gas temperature, density, and extinction for external and internal radiation are specified. The distributions of the temperature, density, and radiation field in a spherically symmetric approximation can be calculated using the radiative transfer model [10], or specified by hand.

The evolution equations of chemical kinetics, including gas-phase reactions, the formation and destruction of ice mantles on dust grains, and surface reactions, are integrated in each cell until a specified age (2×10^6 yr in our study). The initial elemental chemical composition we used is provided in Table 1. We considered initial compositions with purely atomic hydrogen and with all the hydrogen being in molecular form. The rates of gas-phase reactions were calculated using the UMIST database [11]. The model includes 582 components and 4524 gas-phase reactions. The surface reactions were mainly taken from [12, 13], supplemented by dimethyl ether and methyl formate synthesis reactions [4]. The model takes into account the tunneling of reagents through barriers during chemical reactions. The diffusion-to-desorption energy ratio was taken to be 0.5. Following [14], we assumed that a fraction ξ of products resulting from each surface reaction did not remain in the mantle, but instead went immediately into the gas phase (reactive desorption).

Table 1. Initial component abundances used in the model, relative to hydrogen

Component	Abundance
C	0.73 (−4)
N	0.214 (−4)
O	0.176 (−3)
F	0.2 (−7)
He	0.14
Si^+	0.3 (−8)
S^+	0.2 (−7)
Cl^+	0.3 (−8)
Na^+	0.3 (−8)
Mg^+	0.3 (−8)
F^+	0.3 (−8)
P^+	0.3 (−8)
Dust	0.2 (−12)

The formation of molecular dust mantles was modeled using a basic value of 0.3 for the sticking coefficient [9], which is multiplied, for each component, by the fraction of specified molecules whose thermal energy does not exceed their desorption energy (for a Maxwell velocity distribution). In addition to reactive desorption, other processes can also result in mantle destruction, such as photodesorption, thermal desorption, and cosmic-ray-induced desorption.

The calculated results for the one-dimensional structure of an object enable us to determine the column densities of molecules at arbitrary distances from the direction toward the object's center, and to compare these with values derived from observations. We consider here the fit between the observations and the model for the direction toward the center of the object. We took the agreement for a specific component to be satisfactory if the difference between the theoretical and observational column densities did not exceed an order of magnitude. Our choice of this criterion was due to both the imperfect interpretation of the observations and uncertainties in the chemical

Table 2. Calculated and observed column densities for TMC-1. The theoretical values are given for $t = 1.15 \times 10^5$ yr. Molecules that do not fit the observations in model [27] are highlighted in bold

Component	Observations	Model TMC-H2-003	Agreement	Model TMC-H2-0	Agreement	Model TMC-H-003	Agreement	Model TMC-H-0	Agreement
CO	8.0 (17)	4.0 (18)	+	4.0 (18)	+	3.6 (18)	+	3.6 (18)	+
HCO^+	8.0 (13)	2.8 (14)	+	2.8 (14)	+	2.1 (14)	+	2.0 (14)	+
H_2CO	5.0 (14)	1.3 (15)	+	6.5 (14)	+	3.1 (15)	+	2.3 (15)	+
H_3CO^+	3.1 (13)	7.8 (12)	+	3.4 (12)	+	2.0 (13)	+	1.5 (13)	+
OH	2.7 (15)	9.5 (15)	+	7.6 (15)	+	8.3 (15)	+	6.5 (15)	+
C_2O	6.0 (11)	5.1 (11)	+	4.1 (11)	+	1.5 (12)	+	1.3 (12)	+
NH_3	2.0 (14)	1.8 (15)	+	1.5 (15)	+	2.4 (15)	−	2.4 (15)	−
N_2H^+	4.0 (12)	6.2 (12)	+	5.4 (12)	+	4.9 (12)	+	4.4 (12)	+
CN	5.0 (13)	1.1 (14)	+	1.1 (14)	+	1.5 (14)	+	1.6 (14)	+
HCN	2.0 (14)	6.8 (14)	+	6.4 (14)	+	1.2 (15)	+	1.2 (15)	+
HNC	2.0 (14)	5.8 (14)	+	5.6 (14)	+	8.7 (14)	+	8.7 (14)	+
$HCNH^+$	2.0 (13)	8.2 (12)	+	7.6 (12)	+	1.5 (13)	+	1.5 (13)	+
HC_3N	1.6 (14)	2.1 (14)	+	2.1 (14)	+	2.0 (14)	+	2.1 (14)	+
HC_5N	5.6 (13)	4.3 (13)	+	3.3 (13)	+	8.2 (13)	+	9.2 (13)	+
HC_7N	1.2 (13)	1.1 (13)	+	4.9 (12)	+	3.0 (13)	+	2.5 (13)	+
HC_9N	8.4 (12)	4.8 (12)	+	6.0 (11)	−	1.4 (13)	+	6.6 (12)	+
C_3N	6.0 (12)	4.7 (12)	+	4.6 (12)	+	6.4 (12)	+	6.8 (12)	+
C_5N	3.0 (11)	1.0 (12)	+	8.2 (11)	+	3.7 (13)	−	6.5 (13)	−
CH	1.5 (14)	5.3 (13)	+	6.9 (13)	+	3.8 (14)	+	5.4 (14)	+
C_2H	6.5 (14)	2.4 (14)	+	2.4 (14)	+	1.5 (15)	+	1.6 (15)	+
C_5H	5.8 (12)	9.6 (12)	+	9.2 (12)	+	1.1 (14)	−	1.4 (14)	−
C_6H	7.5 (12)	6.1 (12)	+	5.8 (12)	+	3.2 (14)	−	4.1 (14)	−
CH_3OH	3.0 (13)	1.9 (14)	+	7.8 (10)	−	9.2 (13)	+	1.8 (11)	−
H_2CCO	6.0 (12)	6.0 (13)	+	5.9 (13)	+	1.3 (14)	−	1.3 (14)	−
C_3H_2	1.1 (14)	3.0 (14)	+	2.9 (14)	+	3.3 (14)	+	4.2 (14)	+
CH_3CCH	6.0 (13)	6.3 (12)	+	6.0 (12)	−	9.9 (13)	+	1.5 (14)	+
C_4H	6.1 (14)	7.5 (13)	+	7.1 (13)	+	9.1 (14)	+	1.1 (15)	+
CH_2CN	5.0 (13)	1.2 (13)	+	1.2 (13)	+	4.6 (13)	+	6.0 (13)	+
CH_3C_4H	1.8 (12)	9.1 (11)	+	8.2 (11)	+	1.5 (14)	−	2.0 (14)	−
C_7H	1.5 (11)	1.2 (12)	+	1.0 (12)	+	5.3 (13)	−	7.0 (13)	−
C_7H_4	3.1 (12)	4.4 (11)	+	4.1 (11)	+	7.8 (13)	−	1.1 (14)	−
C_8H	4.6 (11)	6.1 (11)	+	5.3 (11)	+	8.9 (13)	−	1.3 (14)	−
CH_2NH	3.6 (13)	1.4 (13)	+	1.1 (13)	+	1.1 (14)	+	8.2 (13)	+
CH_3CHO	6.0 (12)	3.6 (12)	+	3.5 (12)	+	5.8 (12)	+	5.3 (12)	+
CH_3CN	6.0 (12)	3.1 (13)	+	3.1 (13)	+	3.5 (13)	+	3.8 (13)	+
HC_3NH^+	1.0 (12)	3.7 (11)	+	3.6 (11)	+	3.7 (11)	+	3.9 (11)	+

Table 2. (Contd.)

Component	Observations	Model TMC-H2-003	Agreement	Model TMC-H2-0	Agreement	Model TMC-H-003	Agreement	Model TMC-H-0	Agreement
CH_3C_3N	4.5 (11)	2.8 (12)	+	2.8 (12)	+	2.6 (12)	+	2.5 (12)	+
CH_3C5N	7.4 (11)	8.4 (10)	+	6.2 (10)	−	1.3 (11)	+	1.0 (11)	+
CS	4.0 (13)	8.1 (13)	+	7.8 (13)	+	6.6 (13)	+	5.9 (13)	+
H_2S	5.0 (12)	2.4 (12)	+	3.4 (11)	−	7.0 (11)	+	1.5 (11)	−
SO	1.0 (14)	3.6 (13)	+	1.4 (13)	+	1.6 (13)	+	9.5 (12)	−
OCS	2.0 (13)	1.1 (13)	+	9.4 (12)	+	1.0 (13)	+	8.4 (12)	+
C_2S	3.4 (13)	1.8 (13)	+	1.8 (13)	+	1.6 (13)	+	1.5 (13)	+
C_3S	1.0 (13)	7.3 (12)	+	7.2 (12)	+	6.9 (12)	+	6.6 (12)	+
SO_2	1.0 (13)	9.6 (12)	+	2.3 (12)	+	7.2 (12)	+	2.9 (12)	+
H_2CS	7.0 (12)	5.3 (13)	+	5.0 (13)	+	5.3 (13)	+	4.3 (13)	+
H_2O	7.0 (14)	2.5 (16)	−	2.5 (16)	−	2.1 (16)	−	2.1 (16)	−
O_2	7.7 (14)	3.2 (17)	−	2.9 (17)	−	2.1 (17)	−	2.0 (17)	−
C_2	5.0 (14)	1.5 (13)	−	1.4 (13)	−	8.8 (13)	+	9.5 (13)	+
NO	3.0 (14)	2.2 (16)	−	1.6 (16)	−	9.6 (15)	−	6.4 (15)	−
C_3O	1.0 (12)	5.1 (13)	−	2.2 (13)	−	5.0 (13)	−	2.3 (13)	−
C_3H	8.0 (11)	7.4 (13)	−	7.3 (13)	−	1.0 (14)	−	1.1 (14)	−
HCOOH	2.0 (12)	8.9 (13)	−	8.9 (13)	−	1.4 (14)	−	1.3 (14)	−
CH_2CHCN	4.5 (13)	1.3 (11)	−	1.3 (11)	−	6.6 (11)	−	1.2 (12)	−
HCS^+	4.0 (12)	5.8 (10)	−	5.3 (10)	−	5.3 (10)	−	4.4 (10)	−

modeling related to our imperfect knowledge of the rate coefficients of many reactions [15, 16].

3. THE TMC-1 REGION OF LOW-MASS STAR FORMATION

We chose a dense region in the well studied cloud TMC-1 as being a characteristic low-mass prestellar object. This region is approximately 140 pc away [17] and is part of the Taurus Molecular Region. The TMC-1 region has been well studied in both the continuum [18] and spectral lines [19]. Observations have shown that the cloud stretches approximately 0.6 pc from Southeast to Northwest [20–22]. Mapping of CS and CCS lines [23, 24] indicates that the cloud is a chain of separate dense clumps (labeled A–E [24]) rather than a single structure. Differences in the molecular distributions in different regions of the cloud, together with an IRAS source identified in the northwestern part, suggest that different star-forming regions in TMC-1 are in different evolutionary stages, ranging from the young southeastern to the evolved northwestern parts [24–26].

We modeled one of these clumps, namely, the starless, dense core D in the notation of [24], also known as the "cyano-polyynes peak." The rich carbon chemistry of this core, and of TMC-1 as a whole, makes this object interesting for astrochemical studies. We compared the model with compiled data on the molecular composition in TMC-1 from [27], which contains the abundances of several dozen molecules, of which 55 were involved in our model (Table 2), enabling us to carry out a fairly full comparison. The data presented in [27] have been used to test chemical models in a one-point approximation in multiple studies (see, e.g., [28]). Although these data are usually provided as relative abundances, they are actually column densities divided by the mean hydrogen column density of 10^{22} cm^{-2} [29]. Thus, these data are quite suitable for testing multipoint models taking into account the nonuniform distribution of matter and temperature in the object.

The physical structure of the core D has not been determined in detail; therefore, we took a simple den-

Table 3. Models considered in this work

Designation	Physical model	Initial state of H	ξ
TMC-H-0	TMC-1	Atomic	0
TMC-H2-0	TMC-1	Molecular	0
TMC-H-003	TMC-1	Atomic	0.03
TMC-H2-003	TMC-1	Molecular	0.03
DR-H2-0	DR21(OH)M	Molecular	0
DR-H2-003	DR21(OH)M	Molecular	0.03
DRS-H2-0	DR21(OH)M with an internal source	Molecular	0
DRS-H2-003	DR21(OH)M with an internal source	Molecular	0.03

sity distribution in the form

$$n = \frac{n_0}{1 + (r/r_0)^\beta}$$

with the $n_0 = 4 \times 10^6$ cm^{-3} (the density of hydrogen nuclei), $r_0 = 5500$ AU, and $\beta = 2.5$. These values are close to those determined for most dense cores in the region of interest [18, 30, 31]. The obtained distribution is shown by the solid line in Fig. 1. The dust temperature was taken to be 10 K throughout the object. In the inner region, the core was assumed to be isothermal, with equal gas and dust temperatures. Since the temperature of the more rarified gas in TMC may be some tens of degrees Kelvin [32], the temperature at the periphery of the core was increased to 50 K (the temperature profile is also shown in Fig. 1). No internal source was included in the model, since the object is considered to be a starless core. We assumed that the cloud is irradiated by an interstellar radiation field with an intensity of 1.8 Draine units [33].

The chemical evolution of the core was modeled over 2×10^6 years for the distributions of physical parameters described above (assumed to be constant). The radial profiles of the molecular abundances for 55 molecules (Table 2) were used to calculate the column densities in the direction toward the center of the object. We considered four modeles: with the initial hydrogen in atomic and molecular form, and with two different values of ξ, namely, zero and 3%. The model designations are presented in Table 3.

Figure 2 shows how the relative numbers of molecules whose column densities agree with the observations change with time. For all four versions of the core, there is an interval of best agreement between the observations and calculated model covering ages from $\sim 3 \times 10^4$ to $\sim 3 \times 10^5$ yrs. However, this area is only weakly expressed in the models in which hydrogen is initially in atomic form, and the maximum agreement does not exceed 70%. The peak for the best fits is much better defined in the models with initally molecular hydrogen, and corresponds to an age of 10^5 yr. The best agreement (83%) is reached in the model with molecular hydrogen and nonzero reactive desorption for an age of 1.15×10^5 yr. This best-fit chemical age agrees, to order of magnitude, with the results of other studies [27, 29, 34, 35].

The molecules whose theoretical column densities agree with the observed values at $t = 1.15 \times 10^5$ yr to within an order of magnitude are marked with a "+" in Table 2. A comparison of the results for the four calculated models indicates that the models with initially atomic hydrogen display worse agreement with the obsevations, mainly due to the overproduction of carbon chains, C_nH, and similar molecules, which are synthesized more efficiently in a medium with a higher abundance of hydrogen atoms.

By and large, the modeling of TMC-1 was quite successful. The calculated results agree with the observatinal data for both simple and more complex organic molecules, such as CH_2CN, CH_3CN, and CH_3CHO. Figure 3 shows the evolution of the column densities of a number of molecules in the model TMC-H2-003, normalized to the observed column densities. All the molecules that agree with the observations according to the adopted criterion can be divided into three groups. The model column densities of molecules of the first group (which are, as a rule, two- or three-atom molecules) do not differ from the observed column densities by more than an order of magnitude over almost the entire considered interval (Fig. 3a). Molecules in the second group (Fig. 3b) show agreement in either the early or late evolutionary stage only (in both cases, including the age of best agreement). Finally, the third group (Fig. 3c) includes molecules whose model column densities agree with the observations only over a relatively short time interval of nearly $t = 10^5$ yr. This group includes

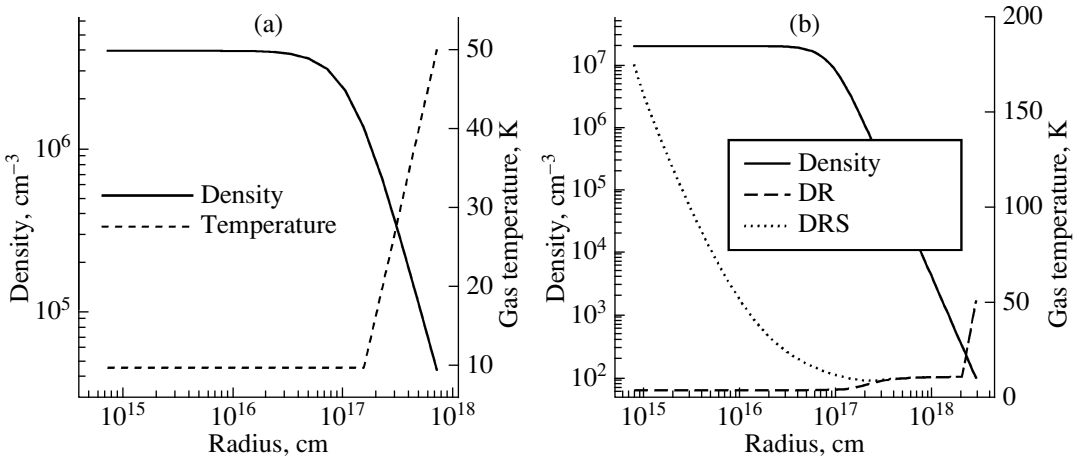

Fig. 1. The density and temperature distributions in the considered models: (a) TMC-1, (b) DR21(OH)M.

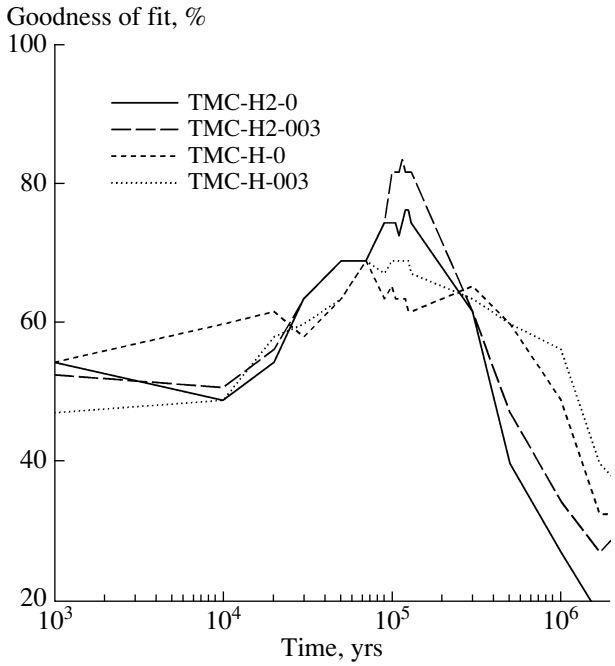

Fig. 2. Fractions of molecules in TMC-1 for which satisfactory agreement with the observations is achieved, as a function of the model age.

almost all the complex compounds, such as CH_2CN, CH_3C_4H, etc.

The age yielding the best agreement is determined by the competition between the synthesis of molecules and the freezing-out of molecules onto dust particles. As was expected, the best agreement for simple molecules is determined by a balance between the "rapid chemistry" of carbon compounds and the "slow chemistry" of nitrogen compounds. However, the position of the peak (i.e., the estimated age of the object) is mainly determined by complex molecules—more precisely, those synthesized in the gaseous phase—rather than simple ones. The beginning of the fitting interval is associated with a slow accumulation of these molecules in the gas (in comparison, e.g., with CO and HCO^+), while the end of this interval corresponds to their gradual passage into ice mantles.

Figure 4 shows separately how the column densities of cyano polyynes, which are considered to be key components of the analyzed region, change over time. The calculated results for these molecules also correspond well to observations until ages of approximately $t = 2 \times 10^5$ yr, after which they decrease due to the

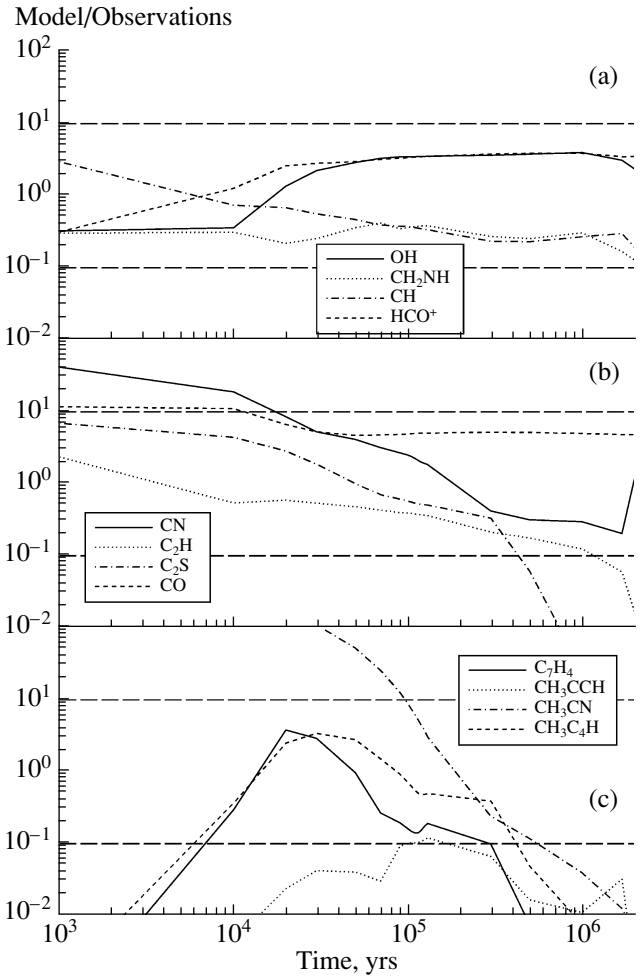

Fig. 3. The ratio of the observed and theoretical column densities for a number of molecrules, as a function of the model age.

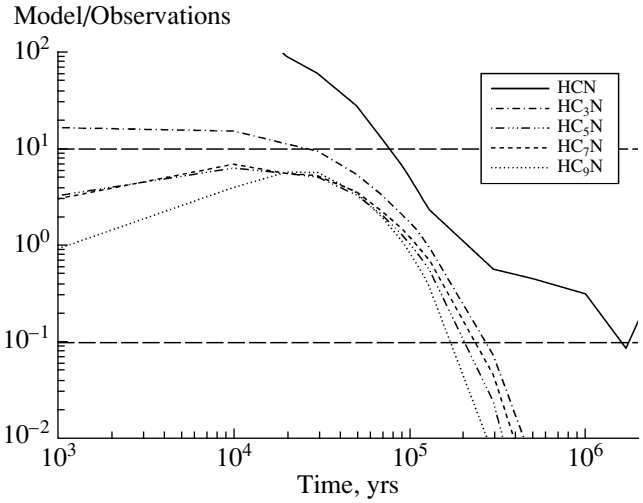

Fig. 4. Ratio of the observed and theoretical column densities for the $HC_{2n+1}N$ molecules, as a function of the model age.

freezing-out of molecules onto dust grains. Accoring to published data, the large number of carbon chains in this region is often explained by an anomalous carbon abundance or a possible recent carbon-rich matter-accretion event. Our model reproduces their abundance without additional assumptions.

Molecules for which agreement with the observations is not reached at all, or is reached at some age beyond the time of best agreement, are by no means less interesting. These molecules are marked with a "–" in Table 2. The origins of these discrepancies are different. For example, the theoretical gas-phase column density of methanol, which is mostly synthesized in surface reactions, is much lower than the observed methanol column density in models with zero reactive desorption. This is obviously due to the fact that thermal desorption and photodesorption are not able to evaporate mantles efficiently at low dust temperature and in the absence of high UV radiation, suggesting that methanol does not pass from the solid into the gas phase. On the other hand, overabundances of water and molecular oxygen can be explained by insufficiently efficient freezing-out of these molecules in our model.

Finally, in some cases, the discrepancies between the observed and theoretical column densities may be due to incompleteness of the grid of chemical reactions used and/or uncertainties in the rate coefficients. The results of adopting a more modern chemical database can be indirectly estimated by comparing our results with the data of [27], where the revised UMIST chemical database was used to study the chemical evolution of TMC-1. Molecules whose column densities could not be fitted to the observations according to [27] are given in bold in Table 2. It is obvious that the abundances of some molecules (in particular, O_2 and H_2O), which are not fit by our model, are successfully reproduced in the model of [27]. The success of the model [27] for water is somewhat tentative: the H_2O abundance has an upper limit of 7×10^{-8}, while the calculated value is 6.9×10^{-7} (the fitting criterion in [27] was also chosen to be a discrepancy no greater than an order of magnitude). However, there are also molecules (in particular, OH and N_2H^+) whose abundances are explained in our model but do not agree with the observations in the model of [27]. In other words, the overall quality of the fitting does not seem to improve unambiguously when utilizing the other database. Of course, it is important to remember that the physical models used in our work and in [27] are appreciably different.

4. DR21(OH)M—COMPLEX MOLECULES IN A MASSIVE PROTOSTELLAR OBJECT

Further, we consider an evolved object that is part of the star-forming region DR21(OH) in the northern part of the Cygnus-X complex at a distance of 1.5 kpc [36]. This region has been studied in both the continuum [37–41] and spectral lines of various molecules [40, 42–45]. The absence of regions of ionized hydrogen [44] indicates that the formation of massive stars in DR21(OH) is in an early stage.

The DR21(OH) region is highly inhomogeneous and contains several cores: M (which, in turn, is divided into MM1 and MM2 [46]), N, W, and S. The cores MM1 and MM2 are the most intense sources with active star-forming processes, as is testified to by the presence of powerful OH [47], H_2O [48], and CH_3OH [49] masers. MM1 is a core with a temperature of approximately 60 K and a mass of $350M_\odot$ [37]. This object is believed to contain at least one pre-main-sequence star [40] that is deeply embedded in a dense gaseous envelope. The second core MM2 is less bright than MM1 at all wavelengths, and is cooler (30 K) and more massive ($570M_\odot$) [37]. This core is believed to contain an early B star [40].

We mostly used the spectral scan data of [50] to compare the model with the observations. We measured the spectrum towards DR21(OH)M at frequencies 84–115 GHz using the radio telescope of the Onsala Space Observatory. An analysis of the measured lines assuming local thermodynamical equilibrium yielded estimates of the column densities of 32 molecules and/or their isotopomers, from simple compounds, such as CO, CS, and HCN, to complex organic molecules, such as CH_3OCHO and CH_3OCH_3. The UMIST database contains 24 of the 32 molecules observed in [50]. A complete list of these molecules together with the column densities obtained in [50] are given in Table 4. If the column density was only available for an isotopomer, this was recalculated to the column density of the molecule containing the major isotope using coefficients of 500 for ^{18}O, 275 for ^{15}N, 60 for ^{13}C, and 23 for ^{34}S. In addition to the column densities given in [50], we estimated the column densities of CH_3OCH_3, CH_3C_3N, and $HCOOCH_3$ using composite spectra, as described in [54]. In addition to the molecules from [50], we also considered column densities of some other components that were measured in DR21(OH)M [43, 51–53].

DR21(OH)M has a complex structure [55], although no detailed information on its temperature and density distributions has been published; only possible ranges or characteristic values of these parameters have been provided (Table 5). To roughly estimate the column densities of various chemical components

Table 4. DR21(OH)M: observational and model column densities calculated for $t = 10^5$ yr

Component	Observations	Model DR-H2-0	Agreement in the model	Model DR-H2-003	Agreement in the model	Model DRS-H2-0	Agreement in the model	Model DRS-H2-003	Agreement in the model	Reference
C^+	1.5 (17)	1.1 (17)	+	1.1 (17)	+	9.9 (16)	+	9.9 (16)	+	[43]
C	5.2 (17)	3.1 (17)	+	3.0 (17)	+	1.5 (17)	+	1.4 (17)	+	[43]
CO	1.6 (19)	2.4 (18)	+	2.5 (18)	+	8.1 (19)	+	8.3 (19)	+	[50]
HCO^+	1.4 (14)	1.5 (14)	+	1.5 (14)	+	6.3 (14)	+	6.3 (14)	+	[50]
H_2CO	2.7 (14)	1.3 (15)	+	1.4 (15)	+	8.4 (14)	+	1.7 (15)	+	[50]
HCO	9.8 (13)	4.8 (13)	+	5.1 (13)	+	1.1 (14)	+	8.6 (14)	+	[50]
H_2CCO	3.5 (13)	6.9 (13)	+	6.7 (13)	+	4.6 (13)	+	4.4 (13)	+	[50]
CS	3.6 (14)	4.7 (13)	+	4.8 (13)	+	6.0 (13)	+	6.1 (13)	+	[50]
OCS	1.8 (14)	2.0 (13)	+	2.5 (13)	+	3.1 (14)	+	3.1 (14)	+	[50]
CN	5.0 (14)	2.7 (14)	+	2.9 (14)	+	2.1 (14)	+	2.2 (14)	+	[50]
HCN	1.8 (14)	7.3 (14)	+	7.3 (14)	+	4.6 (14)	+	4.8 (14)	+	[50]
HNC	1.7 (14)	5.2 (14)	+	5.2 (14)	+	3.6 (14)	+	3.7 (14)	+	[50]
H_2CCC	4.0 (12)	1.8 (13)	+	1.8 (13)	+	1.5 (13)	+	1.4 (13)	+	[50]
HC_3N	1.0 (14)	9.1 (13)	+	9.6 (13)	+	5.4 (13)	+	5.2 (13)	+	[50]
CH_2NH	5.2 (13)	5.6 (12)	+	7.4 (12)	+	8.5 (12)	+	1.6 (13)	+	[50]
CH_3C_3N	1.0 (12)	3.5 (12)	+	3.4 (12)	+	1.3 (12)	+	1.2 (12)	+	[50]
SiO	2.1 (13)	7.1 (13)	+	8.3 (13)	+	7.9 (14)	−	7.9 (14)	−	[50]
HCOOH	4.0 (13)	1.2 (14)	+	1.3 (14)	+	6.1 (14)	−	6.3 (14)	−	[50]
HCl	1.0 (14)	5.4 (12)	−	5.9 (12)	−	2.2 (14)	+	2.2 (14)	+	[51]
C_3H_2	7.4 (13)	8.8 (14)	−	1.0 (15)	−	6.8 (14)	+	7.1 (14)	+	[50]
NH_3	1.8 (16)	6.5 (14)	−	7.9 (14)	−	2.7 (15)	+	3.4 (15)	+	[52]
SO	8.6 (14)	3.7 (13)	−	6.4 (13)	−	9.3 (13)	+	1.3 (14)	+	[50]
$HCOOCH_3$	3.0 (13)	1.1 (08)	−	8.0 (08)	−	4.6 (08)	−	9.9 (13)	+	[50]
N_2H^+	9.2 (13)	4.1 (12)	−	4.8 (12)	−	8.2 (12)	−	9.7 (12)	+	[50]
NS	5.1 (13)	2.7 (11)	−	6.0 (11)	−	1.7 (11)	−	5.9 (12)	+	[50]
C_3	2.2 (14)	2.4 (16)	−	2.2 (16)	−	1.1 (16)	−	1.0 (16)	−	[53]
C_2H	3.6 (15)	2.8 (14)	−	2.7 (14)	−	2.9 (14)	−	2.9 (14)	−	[50]
H_2CS	2.3 (15)	1.8 (13)	−	1.8 (13)	−	1.0 (14)	−	1.0 (14)	−	[50]
CH_3OH	5.2 (15)	3.1 (13)	−	8.0 (13)	−	6.9 (13)	−	4.7 (14)	−	[50]
CH_2CHCN	7.0 (12)	1.4 (10)	−	1.3 (10)	−	1.7 (10)	−	1.6 (10)	−	[50]
HCS^+	1.2 (13)	3.1 (10)	−	3.2 (10)	−	3.7 (10)	−	4.0 (10)	−	[50]
CH_3OCH_3	6.0 (13)	4.7 (09)	−	2.3 (10)	−	1.7 (10)	−	9.3 (10)	−	[50]

in DR21(OH)M, we used a simple, spherically symmetric model, which should be considered in this case as a set of points along the line of sight, rather than an actual representation of the object's geometry, with physical parameters varied at the model points within the ranges characteristic of DR21(OH)M.

Table 5. Sample parameters for the massive protostellar object DR21(OH)M based on various observations

Designation	Surface density, cm^{-2}	Bulk volume density, cm^{-3}	Mass, $M_\odot$	Reference
DR21(OH)M	7×10^{24}	1.1×10^7	4300	[39]
DR21(OH)MM1 + MM2	10^{25}	5×10^7	~1000	[40]
DR21(OH)M	3.3×10^{24}	3.9×10^6	2100	[56]
N44, DR21(OH)	–	10^6	446	[57]
DR21(OH)	2.6×10^{23}	–	1814	[43]

We considered two sets of models (Table 3). The DR models assumed that the object is fully starless, and the dust is heated only by the external radiation field. The DRS models assumed that the dense part of the object is irradiated by a protostar with an effective temperature of 10 000 K. The adopted temperature and density distributions are shown in Fig. 1: the dust temperature in the DRS models was varied from 170 K in the inner region to 12 K at the outer boundary. In the DR models, the cloud remains cold everywhere. The gas temperature was taken to be equal to the dust temperature everywhere except at the outer envelope, where the gas temperature was artificially increased to 50 K. In all cases, the density was varied from 2×10^7 cm^{-3} at the center of the model object to 100 cm^{-3} at its boundary. These distributions correspond to a column density of 2×10^{24} cm^{-2} and a mass of 500 $M_\odot$. The initial abundances of the chemical components were the same as those used while modeling TMC-1. Further, we only present the modeling results for the calculations assuming the initial hydrogen to be entirely in molecular form, since the models with initially atomic hydrogen were less satisfactory for this object, as was also the case for TMC-1. We considered models with zero reactive desorption (the H20 models) and with 3%-efficient reactive desorption (the H2003 models).

A comparison of the model and observed column densities is provided in Fig. 5. The best agreement between the observed and calculated data corresponds to an age of approximately 10^5 yr for DR21(OH)M, as for TMC-1. More precisely, the best agreement is reached for an age of $\sim 8 \times 10^4$ yr in the DR models (18 of 32 component satisfactorily fitted) and an age of $\sim 1.2 \times 10^5$ yr in the DRS models. The DRS-H2-003 model with reactive desorption seems to provide the best fit (23 of 32 components satisfactorily fitted); this is shown by the dotted curve in Fig. 5.

A complete list of all the components considered is given in Table 4, where the separate blocks show components for which agreement with observations was achieved for both groups, only one group, or neither group. As for TMC-1, the model is able to reproduce the observed column densities of both simple and complex components, of carbon, nitrogen, sulphur, and chlorine compounds, and of components with high and low abundances (the column-density range covers six orders of magnitude).

The molecules in the considered list can be divided into a) molecules whose evolution depends on neither the presence of the central source nor the value of ξ; b) molecules whose evolution depends on the presence of the central source but not on the value of ξ; and c) molecules whose evolution depends on both these factors. It is obvious that the first group includes components whose column densities are mainly determined by gas-phase reactions in the outer regions of the cloud. The second group is comprised of components whose column densities depend on gas-

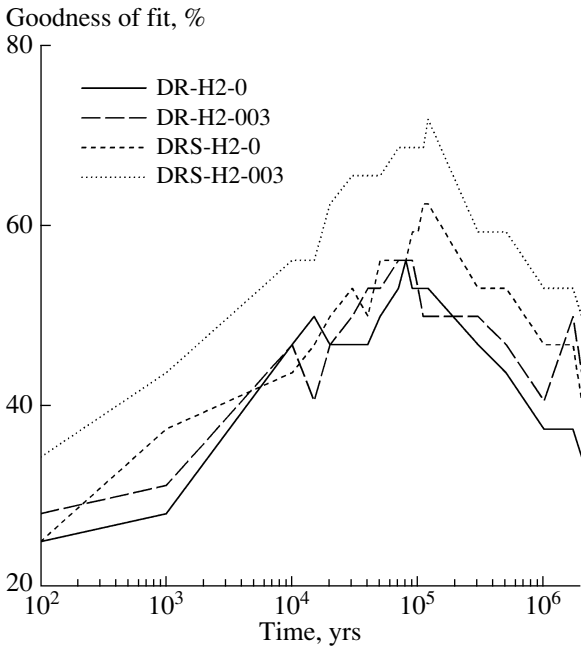

Fig. 5. Fractions of molecules in the DR21(OH)M models that agree with the observations, as a function of the model age.

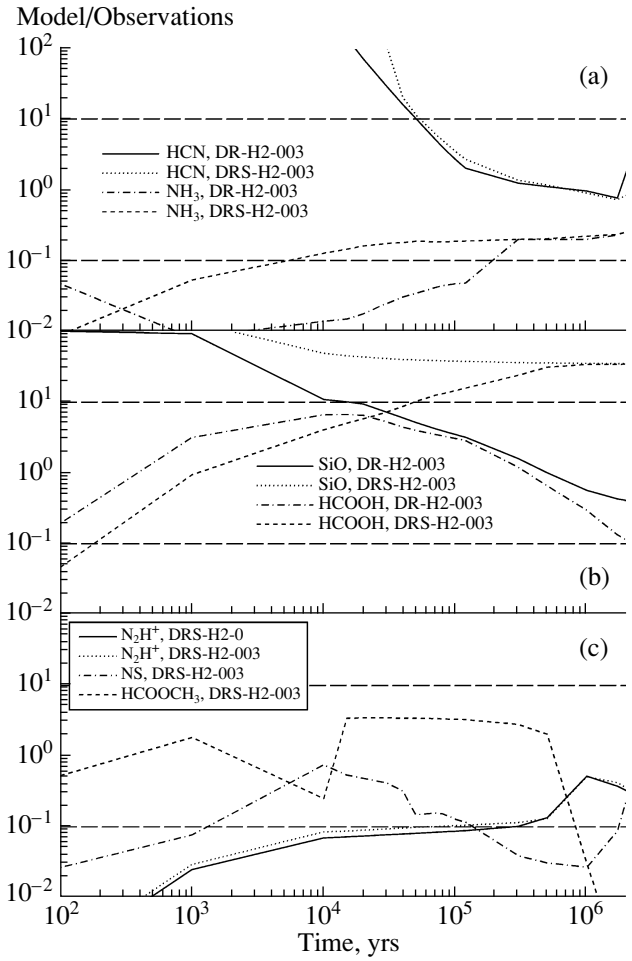

Fig. 6. Ratio of the observed and theoretical column densities as a function of the age of DR21(OH)M for some molecules.

phase reactions in the inner, hot region of the cloud near the protostar. The third group consists of components that form at dust-grain surfaces and enter the gas phase due to reactive and/or photodesorption.

Figure 6a shows the time dependence of the column densities of HCN and NH_3, which are typical of the first and second groups (the results are shown for $\xi = 0.03$, since these column densities depend only weakly on ξ). In addition to HCN, atomic and ionized carbon and some nitrogen compounds (CN, HNC, HC_3N, CH_3C_3N, etc.) also demonstrate a low sensitivity to the model parameters. The ammonia column density in the DR models (dash-dotted curve) grows slowly, and fall within the observed range after $t \approx 2 \times 10^5$ yr only. Ammonia forms more rapidly in the DRS models, due to the high temperature of the gas in the central region. The region of enhanced ammonia abundance begins to appreciably contribute to the total column density starting at earlier times of approximately 3×10^3 yr (Figs. 6a, 7a). The enhanced dust temperature in the DRS models also reduces the efficiency of ammonia freeze-out, suggesting that the gas-phase ammonia abundance remains higher than in the DR models at later times also. However, this higher abundance is only observed in a small volume of the core, due to the high desorption energy of NH_3, and does not contribute appreciably to the total column density of these molecules. In addition to ammonia, this behavior is also characteristic of CO, HCO^+, formaldehyde, and other molecules.

The situation for HCN is somewhat different (Figs. 6a, 7a). At earlier times, the column density of these molecules significantly exceeds the observed value in both groups of models, but the gas-phase HCN abundance begins to decrease with time. This is due purely to the freeze-out of molecules onto dust grains in the DR model, while the freeze-out in the DRS models is only efficient at distances of more than 10^{16} cm from the central source. Photodissociation becomes more appreciable at smaller distances to the core center, affecting the HCN abundance more strongly than the ammonia abundance. The products of ammonia photodissociation (NH, NH_2, and NH_3^+) return to the ammonia synthesis chain, whereas the

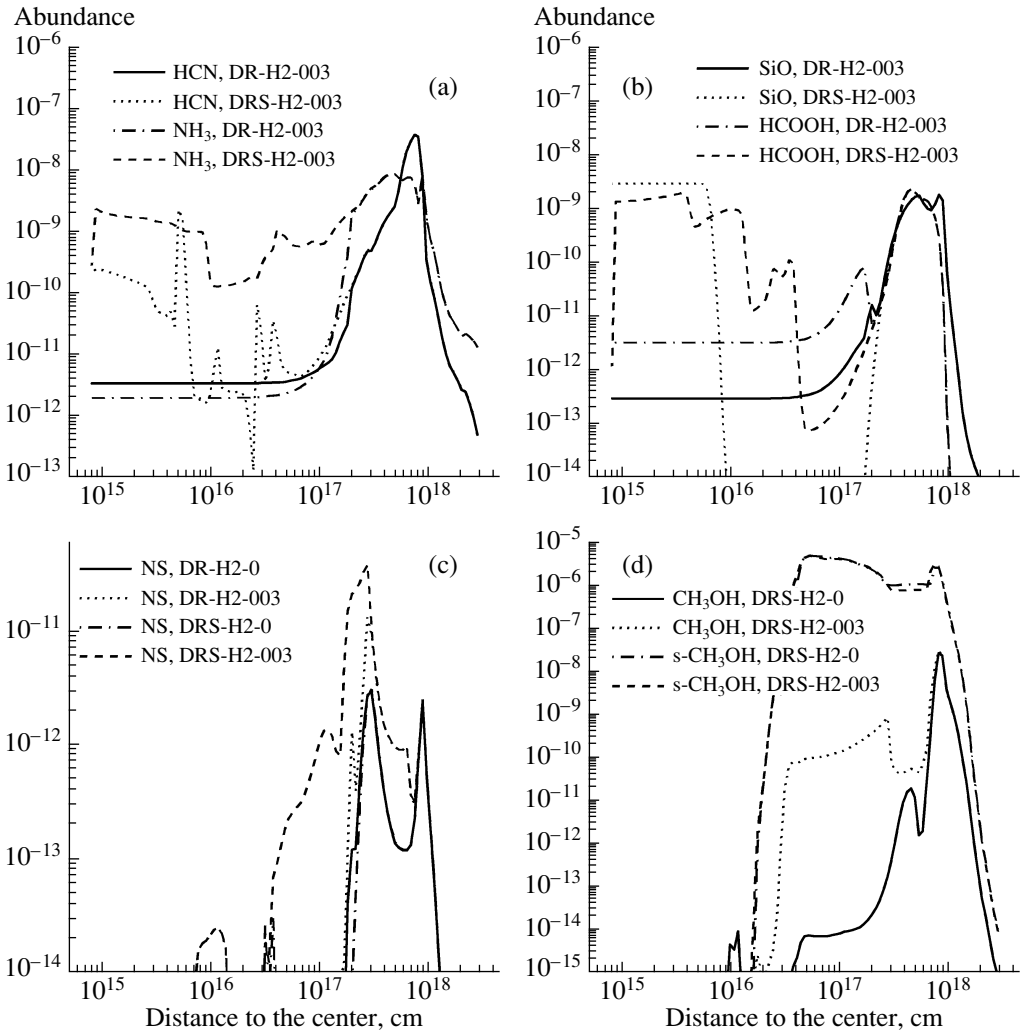

Fig. 7. Radial profiles of the relative abundances of some molecules in the DR21(OH)M models for an age of $t = 1.2 \times 10^5$ yr.

CN radical, which arises in HCN photodissociation, is able to react with O_2 to produce OCN, which reacts with oxygen, yielding CO, CO_2, and NO. As a result, some N atoms pass from HCN to NO, implying that the gas-phase HCN abundance in the DRS models is lower than in the DR models at $t = 10^5$ yr. However, this difference does not contribute appreciably to the total column density, as is also the case with ammonia.

If the molecular column density agrees with the observations in the DRS models but not the DR models, this implies that the column density has increased to an "acceptable" level due to an enhanced molecular abundance in the neighborhood of the protostar, due to either more efficient gas-phase reactions or photodesorption from the surfaces of dust grains. There are only two examples when a discrepancy between the model and observations arises in the presense of a protostar, rather than its absence. Figure 6b shows the evolution of the column densities of SiO and HCOOH, which only show agreement with the observations for the DR models. The SiO and HCOOH abundances in the central cells are substantially enhanced in the DRS models over the entire calculated time (Fig. 7b), resulting in extremely high column densities. In the DR models, SiO and HCOOH freeze out onto dust grains, reducing the column density to an "acceptable" level.

The column densities of N_2H^+, NS, and $HCOOCH_3$ agree with the observed values only in models with a protostar and reactive desorption. A comparison of the model and observed column densities of N_2H^+ (Fig. 6c) highlights the arbitrariness of the adopted fitting criterion. At $t = 10^5$ yr, the column density of N_2H^+ is near the boundary of the adopted interval for both the DRS-H2-0 and DRS-H2-003 models. Formally, agreement is reached only in the model with reactive desorption; however, it is obvious that the DRS-H2-003 model is only

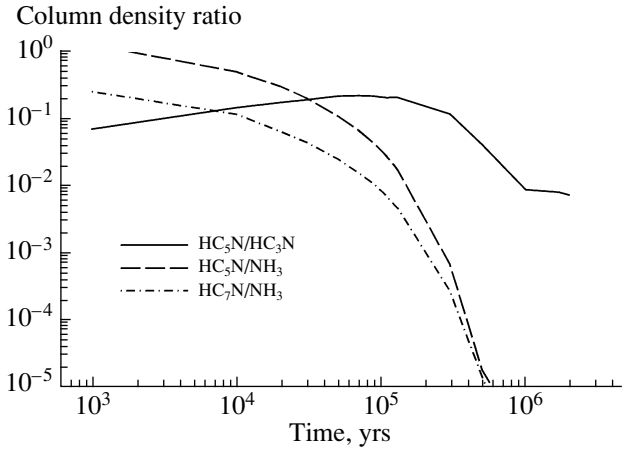

Fig. 8. Ratios of the column densities of some molecules in the TMC-H2-003 model, as a function of the model age.

marginally preferred, since the column densities differ only slightly in the two cases.

A consideration of NS and $HCOOCH_3$ proves critical in models with reactive desorption (Figs. 6c, 7c). An important contribution to the abundances of these components is provided by surface reactions, which are more efficient in the DRS models due to the high dust temperature in the central part of the cloud. Reactive desorption must be added to the model; otherwise, the surface-reaction products are not able to pass to the gaseous phase.

Finally, the results for seven components—C_3, C_2H, H_2CS, CH_3OH, CH_2CHCN, HCS^+, and CH_3OCH_3—do not fit the observations in either model for $t \sim 10^5$ yr: apart from C_3, their column densities remain lower than the observed values during most or all of the calculated time. In particular, the column density of C_2H agrees with the observational results only at times earlier than 10^4 yr, after which it becomes more than an order of magnitude lower than the observed value. However, this discrepancy remains small until a time of approximately 3×10^5 yr. It is thus obvious that this discrepancy can be eliminated through a slight correction in the model parameters, e.g., a small decrease in the desorption temperature for this molecule or an increase in the temperature of the central source. The same is also partly true for methanol, although only in the DRS-H2-003 model, in which the column densities of these molecules are slightly beyond the adopted fitting criterion for 1.2×10^5 yr. The effect of reactive desorption is illustrated in Fig. 7d, which compares the radial profiles of the gas-phase and surface abundances of methanol in the DRS-H2-0 and DRS-H2-003 models (surface components are marked by the prefix "s-"). Reactive desorption with a 3% efficiency is sufficient to enhance the methanol abundance by several orders of magnitude for distances from 3×10^{16} cm to 3×10^{17} cm.

Consistent results for methanol can be achieved if we take a slightly higher value of ξ, since the surface abundances of methanol greatly exceed its abundance in the gas phase in both models. At 1.2×10^5 yr, the column density of s-CH_3OH in the DRS-H2-003 model is 9.6×10^{18} cm^{-2}, which greatly exceeds the observed value. In this model, the enhanced dust temperature also results in the efficient surface synthesis of acrylonitrile and dimethyl ether; however, the column density of s-CH_2CHCN (1.5×10^{12} cm^{-2}) remains lower than the observed value, while the column density of s-CH_3OCH_3 (3.3×10^{14} cm^{-2}) exceeds the observed value only slightly. It is obvious that reactive desorption with an efficiency of a few percent does not solve the problem of the low gas-phase abundances of these molecules. Desorption may be partly due to an outflow, whose presence was suggested in [58].

Recall that we have considered here a stationary model, in which the physical structure of the object does not change over time. It is possible that the gas-phase abundances of some molecules could be raised by the required amount in the stage of hot-core formation in an evolutionary model with the photodesorption of ice mantles. Neither surface reactions nor freeze-out can explain the low abundances of H_2CS and HCS^+ in the models considered. This may be due to incompleteness of the chemical databases used, which do not include all the required reactions involving sulfur-containing compounds.

5. DISCUSSION AND CONCLUSION

Up to now, studies of protostellar objects with various masses has been mostly focused on simple molecules that have been identified in the millimeter and cantimeter bands. The abundances of these molecules have been determined using a small number of chemical reactions that do not present problems in modeling. On the other hand, these molecules (particularly CO and HCO^+) are not very diagnostically helpful for the early stages of protostellar evolution [9]. Therefore, it is necessary to also consider more complex compounds whose abundances depend more strongly on the physical conditions of the model, a chosen set of chemical reactions (including surface reactions), and the elemental composition of the medium, e.g., the C/O ratio.

In this work, we have evaluated the ability of a "typical" multi-point astrochemical model to predict the abundances of complex molecules in protostellar objects with various physical parameters and in various stages of star formation. The results we have

obtained for TMC-1 generally agree with those of earlier studies. However, we must bear in mind that we have considered only the object as a whole when searching for the best-fit column densities, without analyzing its structure. More detailed studies may reveal additional aspects of interest. One of these concerns the discrepancy between our modeling results for the evolution of water and the data of [27], noted above. The relative water abundance in our model does not exceed 10^{-8} in the inner part of the model core, where the physical conditions are similar to those used in [27], that is, it agrees with "representative" values of [27]. However, the column density becomes much higher than the observed value if we take into account the outer envelope, which contains much more water. It is obvious that detailed models of the object's structure and radiative transfer in various spectral lines are required in order to analyze the status of TMC-1 in more detail.

Another remark concerns the chemical inhomogeneity of TMC-1 and other cold cores. The HC_5N/NH_3 ratios in different objects can differ by two orders of magnitude, while the HC_5N/HC_3N ratios in prestellar cores are almost constant ([2]; see also the references therein). Moreover, the difference in the HC_7N/NH_3 ratios can reach factors of several tens, even in TMC-1. Possible origins of these discrepancies can be identified using Fig. 8, which shows the column-density ratios for these molecules as functions of time in the TMC-H2-003 model. It is obvious that the evolution of HC_3N is similar to that of HC_5N (Fig. 4), suggesting that the ratio of their column densities should depend only slightly on time. The evolution of HC_7N proceeds in a similar way. On the contrary, the column density of ammonia remains nearly constant after $t \approx 3 \times 10^4$ yr. The ratios of HC_5N/NH_3 and HC_7N/NH_3 drop by several orders of magnitude over a relatively short time in the vicinity of the time yielding the best agreement, due to the freeze-out of cyanopolyynes. Therefore, the noted differences in the chemical compositions of cold cores could be due to slight differences in their ages. The age gradient mentioned in the Introduction is consistent with this possibility: the HC_7N/NH_3 ratio decreases along the main axis of the cloud, from the Southeast to the Northwest [59]. Moreover, our model does not require any additional assumptions about anomalous an C/O ratio or the accretion of matter enriched with atomic carbon [2].

The application of our model to DR21(OH)M indicates that the model can also yield reasonable results for evolved objects. In spite of the fact that we adopted a physical structure that is fairly arbitrary, the model was able to reproduce the column densities of more than 70% of the molecules studied. The modeling results are consistent with the possibility that the core of DR21(OH)M is in a transitional stage between a starless core and a protostellar object. Analysis of the evolution of various components indicates that the structure of DR21(OH)M reveals signs of both the first and second stages. The column densities of most molecules can be reproduced both in the DR and DRS models. Formally, the DRS model, in which an object has already begun to warm inside, proves to be the best. The discrepancy between our results and the observations is partly due to the fact that the required amounts of some molecules, in particular, dimethyl ether and methyl formate, persist on dust grains, rather than in the gas phase. This suggests that a warm-up phase should be included in the model, in order for sufficient quantities of organic compounds to be accumulated in ice mantles, and then to be converted to the gas phase. We intend to do this in further studies. Another possibility that has been considered recently [60] is that complex organic molecules are eventually formed in gas-phase reactions, but from reagents that have been produced on dust grains and ejected into the gas due to reactive desorption.

The fitting criterion that we have used is not very rigorous, since it admits discrepancies of up to an order of magnitude. This criterion is justified by the uncertainties that arise when recalculating the observed line intensities to column densities. However, the applied physical model enables more reasonable comparisons based on theoretical modeling of spectral line profiles. We cannot rule out the possibility that some of our results could change. Specifically, the radial distribution of CO throughout the cloud has two peaks in the DRS model—at the outer boundary and in the central part of the cloud. Their weights to the column density are equal, but the line-excitation conditions in these two regions differ strongly, implying that their contributions to the CO(1–0) intensity should be substantially different. Only modeling of the radiative transfer can help in addressing this problem. The model we have presented can serve as a good base for such studies.

ACKNOWLEDGMENTS

This work was supported by the Russian Foundation for Basic Research (projects 10-02-00612 and 13-02-00642), and the Federal Targeted Program "Research and Scientific–Pedagogical Staff of Innovational Russia" for 2009–2013 (state contract 14.B37.21.0251).

The authors thank Ya.N. Pavlyuchenkov for providing us with the program used to model the radiative transfer and dust temperatures. A.I.V. thanks the National Science Foundation (USA) for its funding

of the astrochemistry program at the University of Virginia.

REFERENCES

1. E. A. Bergin and W. D. Langer, Astrophys. J. **486**, 316 (1997).
2. E. Herbst and E. F. van Dishoeck, Ann. Rev. Astron. Astrophys. **47**, 427 (2009).
3. R. Garrod and E. Herbst, Astron. Astrophys. **457**, 927 (2006).
4. R. T. Garrod, S. L. Widicus Weaver, and E. Herbst, Astrophys. J. **682**, 283 (2008).
5. A. I. Vasyunin and E. Herbst, Astrophys. J. **762**, id. 86 (2013).
6. D. S. Wiebe, V. I. Shematovich, and B. M. Shustov, Astron. Rep. **40**, 639 (1996).
7. V. I. Shematovich, B. M. Shustov, and D. S. Wiebe, Mon. Not. R. Astron. Soc. **292**, 601 (1997).
8. V. I. Shematovich, D. S. Wiebe, and B. M. Shustov, Astron. Rep. **43**, 645 (1999).
9. Ya. Pavlyuchenkov, D. Wiebe, R. Launhardt, and Th. Henning, Astrophys. J. **645**, 1212 (2006).
10. Ya. N. Pavlyuchenkov, D. S. Wiebe, A. M. Fateeva, and T. S. Vasyunina, Astron. Rep. **55**, 1 (2011).
11. J. Woodall, M. Agundez, A. J. Markwick-Kemper, and T. J. Millar, Astron. Astrophys. **466**, 1197 (2007).
12. T. I. Hasegawa, E. Herbst, and C. M. Leung, Astrophys. J. Suppl. Ser. **82**, 167 (1992).
13. T. I. Hasegawa and E. Herbst, Mon. Not. R. Astron. Soc. **261**, 83 (1993).
14. R. T. Garrod, V. Wakelam, and E. Herbst, Astron. Astrophys. **467**, 1103 (2007).
15. A. I. Vasyunin, A. M. Sobolev, D. S. Wiebe, and D. A. Semenov, Astron. Lett. **30**, 566 (2004).
16. A. I. Vasyunin, D. Semenov, Th. Henning, et al., Astrophys. J. **672**, 629 (2008).
17. J. H. Elias, Astrophys. J. **224**, 857 (1978).
18. S. Schnee and A. Goodman, Astrophys. J. **624**, 254 (2005).
19. N. Kaifu, M. Ohishi, and K. Kawaguchi, Publ. Astron. Soc. Jpn. **56**, 69 (2004).
20. E. Churchwell, G. Winnewisser, and C. M. Walmsley, Astron. Astrophys. **67**, 139 (1978).
21. L. T. Little, P. W. Riley, and G. H. MacDonald, Mon. Not. R. Astron. Soc. **183**, 805 (1978).
22. A. Wootten, E. P. Bozyan, and D. B. Garrett, Astrophys. J. **239**, 844 (1980).
23. R. L. Snell, W. D. Langer, and M. A. Frerking, Astrophys. J. **255**, 149 (1982).
24. Y. Hirahara, H. Suzuki, and S. Yamamoto, Astrophys. J. **394**, 539 (1992).
25. L. T. Little, G. H. MacDonald, and P. W. Riley, Mon. Not. R. Astron. Soc. **189**, 539 (1979).
26. M. Guelin, W. D. Langer, and R. W. Wilson, Astron. Astrophys. **107**, 107 (1982).
27. D. McElroy, C. Walsh, A. J. Markwick, et al., Astron. Astrophys. **550**, A36 (2013).
28. D. Semenov, D. Wiebe, and Th. Henning, Astron. Astrophys. **417**, 93 (2004).
29. M. Ohishi, W. M. Irvine, and N. Kaifu, Proc. IAU Symp. **150**, 171 (1992).
30. W. D. Langer, T. Velusamy, T. B. H. Kuiper, et al., Astrophys. J. **453**, 293 (1995).
31. M. Tafalla, P. C. Myers, P. Caselli, et al., Astrophys. J. **569**, 815 (2002).
32. P. F. Goldsmith, Astrophys. J. **557**, 736 (2001).
33. B. T. Draine, Astrophys. J. Suppl. Ser. **36**, 595 (1978).
34. H. Roberts and E. Herbst, Astron. Astrophys. **395**, 233 (2002).
35. S. Schnee, P. Caselli, A. Goodman, et al., Astrophys. J. **671**, 1839 (2007).
36. K. L. J. Rygl, A. Brunthaler, A. Sanna, et al., Astron. Astrophys. **539**, id. A79 (2012).
37. E. D. Araya, S. Kurtz, and P. Hofner, Astrophys. J. **698**, 1321 (2009).
38. K. J. Richardson, G. J. White, and J. P. Phillips, Mon. Not. R. Astron. Soc. **219**, 167 (1986).
39. K. J. Richardson, G. Sandell, and K. Krisciunas, Astron. Astrophys. **224**, 199 (1989).
40. J. G. Mangum, A. Wootten, and L. G. Mundy, Astrophys. J. **378**, 576 (1991).
41. J. P. Vallé and J. D. Fiege, Astrophys. J. **636**, 332 (2006).
42. K. J. Richardson, G. Sandell, and C. T. Cunningham, Astron. Astrophys. **286**, 555 (1994).
43. H. Jakob, C. Kramer, R. Simon, et al., Astron. Astrophys. **461**, 999 (2007).
44. T. Hezareh, M. Houde, and C. McCoey, Astrophys. J. **684**, 1221 (2008).
45. N. Schneider, T. Csengeri, and S. Bontemps, Astron. Astrophys. **520**, id.A49 (2010).
46. D. P. Woody, S. L. Scott, N. Z. Scoville, et al., Astrophys. J. Lett. **337**, L41 (1989).
47. R. P. Norris, R. S. Booth, and P. J. Diamond, Mon. Not. R. Astron. Soc. **201**, 191 (1982).
48. R. Genzel and D. Downes, Astron. Astrophys. **30**, 145 (1977).
49. W. Batrla and K. M. Menten, Astrophys. J. Lett. **329**, L117 (1988).
50. S. V. Kalenskii and L. E. B. Johansson, Astron. Rep. **54**, 295 (2010).
51. R. Peng, H. Yoshida, R. A. Chamberlin, et al., Astrophys. J. **723**, 218 (2010).
52. J. G. Mangum, A. Wootten, and L. G. Mundy, Astrophys. J. **388**, 467 (1992).
53. B. Mookerjea, G. E. Hassel, M. Gerin, et al., Astron. Astrophys. **546**, A75 (2012).
54. S. V. Kalenskii and L. E. B. Johansson, Astron. Rep. **54**, 1084 (2010).
55. L. A. Zapata, L. Loinard, Y.-N. Su, et al., Astrophys. J. **744**, 86 (2012).
56. C. J. Chandler, W. K. Gear, and R. Chini, Mon. Not. R. Astron. Soc. **260**, 337 (1993).
57. F. Motte, S. Bontemps, P. Schilke, et al., Astron. Astrophys. **476**, 1243 (2007).
58. E. D. Araya, S. Kurtz, P. Hofner, and H. Linz, Astrophys. J. **698**, 1321 (2009).
59. C. A. Olano, C. M. Walmsley, and T. L. Wilson, Astron. Astrophys. **196**, 194 (1988).
60. A. I. Vasyunin and E. Herbst, Astrophys. J. **769**, id. 34 (2013).

Translated by N. Lipunova